

Performance Evaluation of Solid Oxide Fuel Cell Engines Integrated With Single/ Dual-Spool Turbochargers

So-Ryeok Oh¹

e-mail: srohum@umich.edu

Jing Sun

e-mail: jingsun@umich.edu

Naval Architecture and Marine Engineering,
University of Michigan,
Ann Arbor, MI 48109

Herb Dobbs

Joel King

U.S. Army TARDEC,
6501 E. 11 Mile Road,
Warren, MI 48397-5000

This study investigates the performance and operating characteristics of 5kW-class solid oxide fuel cell and gas turbine (SOFC/GT) hybrid systems for two different configurations, namely single- and dual- spool gas turbines. Both single and dual spool turbochargers are widely used in the gas turbine industry. Even though their operation is based on the same physical principles, their performance characteristics and operation parameters vary considerably due to different designs. The implications of the differences on the performance of the hybrid SOFC/GT have not been discussed in literature, and will be the topic of this paper. Operating envelopes of single and dual shaft systems are identified and compared. Performance in terms of system efficiency and load following is analyzed. Sensitivities of key variables such as power, SOFC temperature, and GT shaft speed to the control inputs (namely, fuel flow, SOFC current, generator load) are characterized, all in an attempt to gain insights on the design implication for the single and dual shaft SOFC/GT systems. Dynamic analysis are also performed for part load operation and load transitions, which shed lights for the development of safe and optimal control strategies. [DOI: 10.1115/1.4004471]

1 Introduction

Solid oxide fuel cells (SOFC), which operate at elevated temperatures ($\sim 800^\circ\text{C}$), are particularly well suited to combine with a gas turbine (GT) as the bottoming cycle in a hybrid SOFC-GT configuration. By integrating the two power plants with complementary characteristics, the efficiency of such a system can potentially exceed 60% and even approach 70% for future optimized designs [1–4].

Various layouts for hybrid SOFC/GT plant have been proposed in the literature. Most of them include combinations of SOFC stacks, heat exchangers, compressor, gas turbines, prereformer, and combustors in different arrangements [2,3]. Most of the SOFC/GT designs replace the gas turbine combustor directly with the fuel cell stack, resulting in the stack being pressurized at the operating pressure of the gas turbine [5]. Other designs, such as the atmospheric SOFC/GT system proposed in Ref. [6] can be also found in literature. It has been shown that the wide range of operation can be supported by burning residue and supplementary fuel in the afterburner. Both simulation and experimental studies show that the steady state efficiency increases substantially for the integrated SOFC/GT systems, compared to their stand-alone SOFC or GT modules [3]. Achieving high efficiency of the SOFC/GT system without compromising system safety and reliability represents a key challenge for control development [9]. Modeling efforts have been reported by various group aimed at facilitating control design and optimization [8].

This paper, built on our previous work [10] which was focused on developing a fast load following scheme, presents a comparative study about the performance capability of two distinct SOFC/GT designs shown in Fig. 1.

One is a single-shaft design with the compressor and turbine mounted on the same shaft as the power generator. Another is a

dual-shaft design with two turbines, namely one drives a compressor and another is a free power turbine driving a generator. While the single- and dual-shaft turbine configurations have been widely employed for SOFC/GT hybrid systems study, to the best of our knowledge, the effects of turbine connection mechanisms on the SOFC/GT operation have not been reported in the open literature. In particular, this paper addresses the following topics: First, the performance capability of the two different SOFC/GT designs is compared in terms of a part-load envelope, system efficiency, and SOFC temperature level. Second, the sensitivity of crucial system parameters on the control variables, namely the fuel flow, SOFC current density, and generator loads, is analyzed and admissible ranges for control variables and advantageous load operation points are identified through model based analysis. Furthermore, applying the derived operation points, the shutdown behavior of the SOFC/GT cycles during load changes is explored through a region of attraction analysis for both single and dual shaft system.

The remainder of this paper is organized as follows: in the next section the system operation principles are presented. SOFC and the gas turbine models are described in Secs. 3 and 4, respectively. Performance evaluations in the steady state and transient are presented in Secs. 5 and 6, respectively, followed by the conclusions.

2 System Operation Principles

The hybrid SOFC/GT system analyzed in this work is intended as an auxiliary power unit (APU) for military and commercial vehicle applications. For example, this unit can be employed in a commercial vehicle to avoid idling of the main engine for power production during stops to improve efficiency. Additionally, it can be used to recharge batteries in the field as well as act as generators. The system is designed to have a rated power of around 5kW. The utility of a dual-shaft gas turbine, shown in Fig. 1(b), is explored in comparison with its single shaft counterpart in achieving efficient steady state operation and smooth transient response for a highly coupled SOFC/GT system. The key system components include an SOFC stack, a compressor (C), a catalytic burner (CB) as the after-burner, turbines (T) which drives a generator

¹Corresponding author.

Contributed by the Advanced Energy Systems Division of ASME for publication in the JOURNAL OF FUEL CELL SCIENCE AND TECHNOLOGY. Manuscript received April 26, 2011; final manuscript received May 8, 2011; published online October 5, 2011. Editor: Nigel M. Sammes.

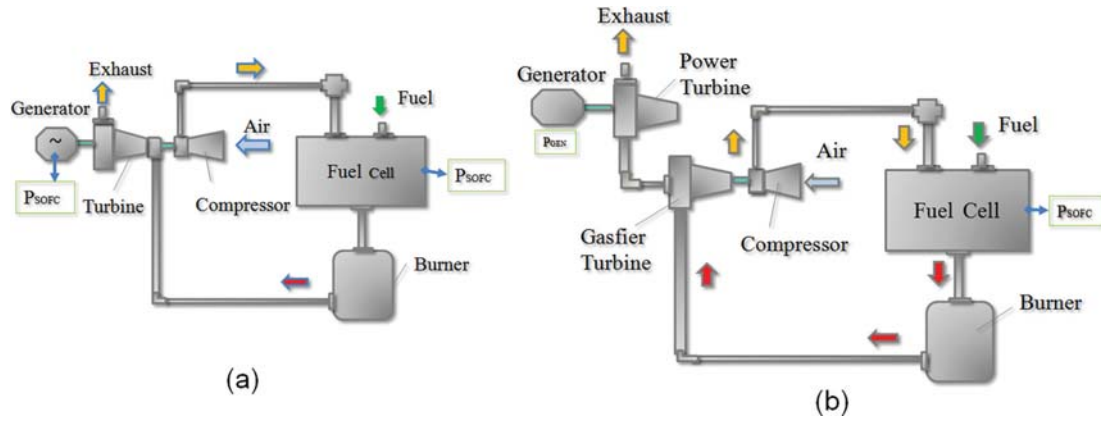


Fig. 1 SOFC/GT Hybrid schematic: single-shaft (a) and dual-shaft (b)

(GEN). Other components, such as the reformer and the heat exchangers, are not included in this work in order to focus on the coupling dynamics between the SOFC and the GT.

The description of the general working principles of the SOFC/GT systems can be found in Ref. [9]. For most of the SOFC/GT systems, the air to the SOFC is supplied to the cathode side by a compressor, while fuel is fed to the anode side. The exhaust from the SOFC outlet passes through the CB where the unused fuel is burned to increase the temperature and pressure of the flow. The high temperature and high pressure flow from the CB then powers the turbine, thereby providing a mechanism to recuperate the exhaust energy. In the single-shaft design (Fig. 1(a)) the turbine drives both the compressor and the generator through a mechanical shaft; the former delivers the air needed for the SOFC stack operation and the latter provides additional electrical power for the system. The net power output is the sum of the electric power from the SOFC and the generator. On the other hand, in the split-shaft design (Fig. 1(b)) there are two turbines. One is a gasifier turbine driving a compressor and another is a free power turbine driving a generator. Since these two turbines have no mechanical coupling, the design can offer better flexibility of operation for the compressor and the power turbine. In the sequel, the modeling of the plant components is explained.

3 SOFC Model Description

SOFC is the key component of the system. In this work, the tubular type SOFC, used in most of SOFC/GT studies due to its advantages in terms of the thermal expansion and gas sealing, is considered and its dynamic model is established.

In a tubular design, air is supplied to the inside of the tube and fuel to the outside (see Fig. 2). Air enters the feed tube at the bottom and travels to the closed end of the cell at the top. Fuel enters on the outside at the closed end. The air and fuel both flow along the cell in the same direction from the closed end toward the open end. This is known as a co-flow configuration.

3.1 Tubular SOFC Model. Our modeling approach takes into account the trade-off between acceptable computational load and sufficient model accuracy. The following modeling strategies have been implemented to reduce the complexity of the resulting model without significant compromise on the accuracy: (1) The anode, cathode, and electrolyte are treated as one single entity. Based on the physical structure of the SOFC, five temperature layers were defined, namely the temperatures for the fuel bulk flow, air bulk flow, positive electrode-electrolyte-negative electrode assembly (PEN), injector, injector air. (2) The fuel is a mixture of six species, consisting of methane(CH₄), carbon monoxide(CO), carbon dioxide(CO₂), hydrogen(H₂), steam(H₂O) and nitrogen(N₂), where the concentration of each species can be var-

ied to reflect different prereforming results. (3) The SOFC can be treated as a distributed parameter system in order to capture the spatial distribution along the flow field for variables such as temperature, species concentration, and current density. The governing equations are described using discretization technique [11]. In this modeling effort, the cell is divided into *n* axial sections (see Fig. 2) and each section is considered as a lumped parameter sub-system.

3.1.1 Electrochemical Model. The operating voltage of one discretization unit of the cell can be calculated as follows:

$$U_j = U_{OCV}^j - (\eta_{ohm}^j + \eta_{act}^j + \eta_{con}^j), \quad j = 1, 2, \dots, n, \quad (1)$$

where *j* is the index of discretization units, as shown in Fig. 2. U_{OCV}^j is the open circuit voltage in the *j*th unit. For simplicity, the superscript *j* will be omitted in the rest of the presentation. The open circuit voltage can be determined by the Nernst Equations as follows:

$$U_{OCV} = E_0 - \frac{\tilde{R}T_{PEN}}{2F} \ln \frac{p_{H_2O}}{p_{H_2} p_{O_2}^{0.5}} \quad (2)$$

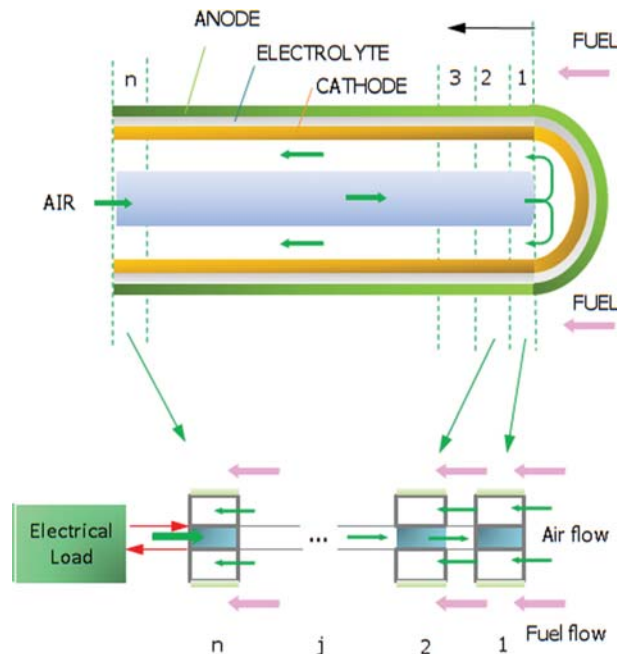


Fig. 2 Finite volume discretization for a tubular SOFC

with $E_0 = 1.2723 - 2.7645 \times 10^{-4} T_{PEN}$ [11], where T_{PEN} is the temperature of the PEN structure, and p_{H_2O} , p_{H_2} , and p_{O_2} are the partial pressures of H_2O , H_2 , and O_2 , respectively. The last three terms in Ref. [1] represents various potential losses: The activation loss, η_{act} , is due to the energy barriers to be overcome in order for the electrochemical reaction to occur, and can be characterized by the Butler-Volmer equation. The concentration loss, η_{con} , reflects the overpotential due to the species diffusion between the reaction site and the bulk flow in gas channels, and η_{ohm} is the ohmic loss due to the electrical and ionic resistance along the path of the current in the fuel cell. The ohmic, activation and concentration polarization are calculated according to the procedure discussed in Ref. [11].

3.1.2 Mass Balances. For the mass balance in the fuel channel, the chemical species considered are CH_4 , H_2O , CO , CO_2 , H_2 , and N_2 , while for the air channel the chemical species are O_2 and N_2 . Table 1 presents the fuel and air channel mass balance equations. In the fuel channel, three reactions are taken into account: methane steam reforming (SR), water gas-shift (WGS), and hydrogen electrochemical oxidation (Ox). In the air channel, only the reduction reaction of O_2 to O^{2-} ions is considered (Red). Table 2 lists all these reactions. According to Faraday's law, the rates of Ox and Red reactions are related to the current density as follows:

$$r_{Ox} = r_{Red} = \frac{i}{2F} \quad (3)$$

The SR reaction is slow and highly endothermic, while the WGS is fast and weakly exothermic. Thus, the entire reforming process is dominated by the endothermic SR reaction that requires the heat generated by the electrochemical reaction. In this study, the model proposed by Ref. [11] is adopted for the reaction rate of the fuel reforming reaction, namely:

$$r_{SR} = 0.04274 \cdot p_{CH_4} \cdot \exp\left(-\frac{E_{SR}}{RT_f}\right) \quad (4)$$

with $E_{SR} = 82 \text{ kJmol}^{-1}$ and all the CO is assumed to be converted through the shift reaction, considered to be at equilibrium [12]. The formula given in Ref. [12] is used to account for this effect:

$$r_{WGS} = k_{WGS} \cdot p_{CO} \cdot \left(1 - \frac{p_{CO_2} p_{H_2}}{p_{CO} p_{H_2O} K_{eq,WGS}}\right) \quad (5)$$

where $k_{WGS} = 0.01$ in this model and $K_{eq,WGS}$ is the equilibrium constant with $K_{eq,WGS} = \exp(4276/T_f - 3.961)$ where T_f is the temperature of the fuel channel.

3.1.3 Energy Balances. The temperatures in five layers, i.e., the fuel/air bulk flow (T_f/T_a), PEN structure (T_{PEN}), the feed tube/air (T_I , T_{Ia}), are calculated by solving the dynamic equations of the energy balance in each layer. The energy balance dynamics are listed in Table 3. Right-hand side (RHS) terms in the equations are composed of rate of energy entering/leaving a control volume by inflow/outflow and rate of heat added/dissipated through both chemical reaction and heat transfer. The heat transfer processes include heat release due to the chemical and electrochemical reac-

Table 1 Dynamic SOFC model: mass balance equation

Location	Reaction	Expression
Fuel channel	SR	$CH_4 + H_2O \rightarrow CO + 3H_2$
	WGS	$CO + H_2O \rightarrow CO_2 + H_2$
Anode	Ox	$H_2 + O^{2-} \rightarrow H_2O + 2e^-$
Cathode	Red	$0.5O_2 + 2e^- \rightarrow O^{2-}$

Table 2 Reactions considered in the model

Location	Reaction	Expression
Fuel channel	SR	$CH_4 + H_2O \rightarrow CO + 3H_2$
	WGS	$CO + H_2O \rightarrow CO_2 + H_2$
Anode	Ox	$H_2 + O^{2-} \rightarrow H_2O + 2e^-$
Cathode	Red	$0.5O_2 + 2e^- \rightarrow O^{2-}$

tions and electrical resistances; convective heat transfer between cell components and fuel and air gas streams; and heat conduction through cell components; radiation heat exchange between the PEN and an air feed tube.

3.2 Dynamic Simulation and Model Validation. A tubular SOFC model was implemented in the Matlab/Simulink environment. The model predicts the various temperatures along the flow path, the gas composition in the fuel and air channel, all the electrochemical-related variables (open-circuit voltage, current density) as well as the cell efficiency and power output. The cell parameters, such as operating conditions and the physical property values of the cell materials and geometry, have taken from the literature [11,13]. The simulations were conducted under the following conditions: the cell inlet temperature is 1000 K, fuel utilization is set to 85%, and air has a stoichiometric ratio of four. Figure 3(a) shows the results of different temperature profiles for the fuel and air channels, PEN structure, and injector, along the

Table 3 Dynamic SOFC model: energy balances

Location	Equation
Fuel channel	$\left(\sum_f \rho_f c_{p,f}\right) \frac{dT_f}{dt} = (q_{in,f} - q_{out,f}) \frac{1}{V} + k_{f,PEN} (T_{PEN} - T_f) \frac{1}{d_f} + r_{Ox} [h_{H_2O}(T_{PEN}) - h_{H_2}(T_f)] \frac{1}{d_f}$ $f \in \{CH_4, CO_2, CO, H_2O, H_2, N_2\}$
Cell Air Channel	$\left(\sum_a \rho_a c_{p,a}\right) \frac{dT_a}{dt} = (q_{in,a} - q_{out,a}) \frac{1}{V} + K_{a,PEN} (T_{PEN} - T_a) \frac{1}{d_a} + K_{a,I} (T_{PEN} - T_a) \frac{1}{h_a} - 0.5r_{Red} h_{O_2}(T_a) \frac{1}{d_a}$ $i \in \{O_2, N_2\}$
PEN structure	$\rho_{PEN} c_{v,PEN} \frac{dT_{PEN}}{dt} = q_{cond,PEN} - k_{f,PEN} (T_{PEN} - T_f) \frac{1}{\tau_{PEN}} + k_{a,I} (T_{PEN} - T_a) \frac{1}{\tau_{PEN}} + r_{Ox} [h_{H_2}(T_f) + 0.5h_{O_2}(T_a) - h_{HO_2}(T_{PEN})] \frac{1}{\tau_{PEN}} - iU + \left[\frac{\sigma(T_I^4 - T_{PEN}^4)}{1/\epsilon_1 + 1/\epsilon_{PEN} - 1} \right] \frac{1}{\tau_{PEN}}$
Injector	$\rho_I c_{v,I} \frac{dT_I}{dt} = q_{cond,Ia} - k_{Ia,I} (T_{Ia} - T_I) \frac{1}{\tau_I} - K_{a,I} (T_{PEN} - T_a) \frac{1}{\tau_I} - \left[\frac{\sigma(T_I^4 - T_{PEN}^4)}{1/\epsilon_1 + 1/\epsilon_{PEN} - 1} \right] \frac{1}{\tau_I}$
Feed Air	$\left(\sum_{Ia} \rho_{Ia} c_{p,Ia}\right) \frac{dT_{Ia}}{dt} = (q_{in,Ia} - q_{out,Ia}) \frac{1}{V} + k_{Ia,I} (T_{Ia} - T_I) \frac{1}{d_{Ia}}$ $Ia \in \{O_2, N_2\}$

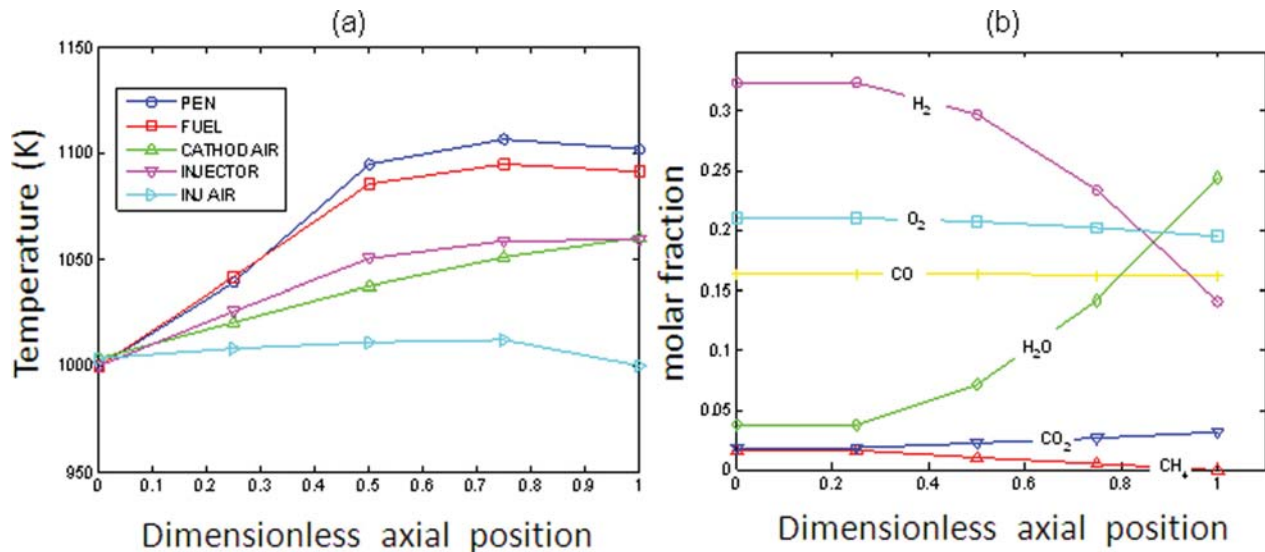


Fig. 3 (a) Fuel and air channels, PEN structure, and injection tube temperature along the cell length. (b) Fuel channel component mole fraction along the cell length.

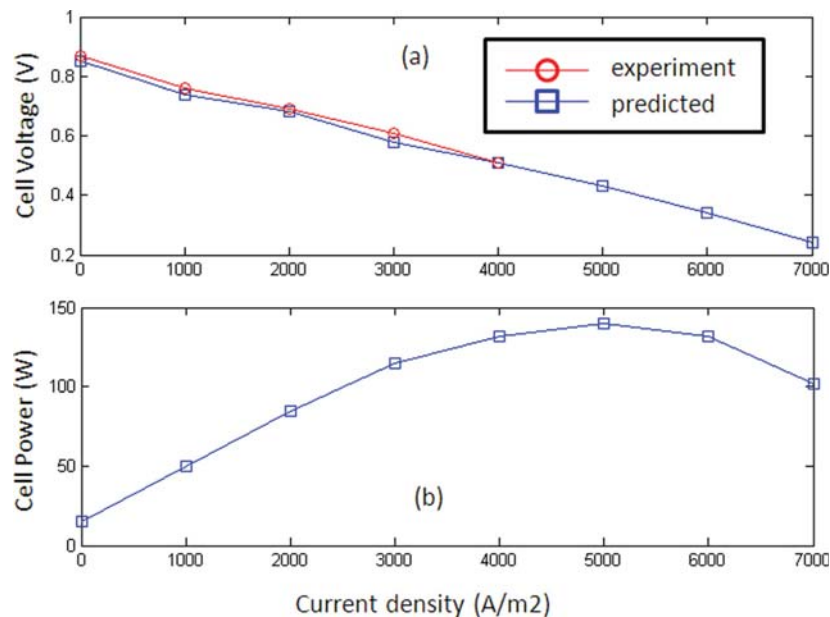


Fig. 4 (a) Comparison between predicted and measured voltage-current density characteristics. An experimental data of a tubular Siemens Westinghouse SOFC presented in Ref. [1] has been used for the fuel cell model verification. (b) The predicted cell power versus current density profile.

flow axis. It can be seen that the cell temperature increases along the fuel and air flow directions with the maximum temperature occurring at the outlet. Figure 3(b) presents the mole fraction profiles in the fuel channel stream. These illustrate the impact of the simultaneous occurrence of the direct internal reforming reaction, the water gas shift reaction, and the oxidation of hydrogen at the anode-electrolyte interface. The consumption of hydrogen and the production of steam can be clearly identified along the cell length as the hydrogen oxidation reaction proceeds. At the exit of the fuel channel, all the methane has been fully consumed and the stream content is 33% in H₂O, 4% in CO, 6% in H₂, and 16% in CO₂.

Figure 4 presents the cell voltage and power density as a function of current density. In Fig. 4(a), the simulation results are compared to the actual test data taken from Ref. [1] for voltage

and power output corresponding to different current density. This comparison shows a good match between the simulation model and the test data (presented in literature) as the percent error between the model prediction and experimental test data is less than 3% over the entire current density range.

In order to combine the tubular SOFC with a gas turbine cycle, the nominal cell operation point has been selected to match the gas turbine system. The cell operating point is often designed to be where the ohmic resistance has a dominant influence. For this tubular SOFC system, this corresponds to a voltage range of 0.6 – 0.7 V. With this voltage range, an average current density of 2000 A/m² and a single cell power of 90 W have been calculated from the cell current power profile shown in Fig. 4(b). The stack was chosen to have 60 cells in order to produce a rated power of 5.4 [kW]. We then chose the fuel flow for the tubular

Table 4 Design point data of the tubular SOFC

Parameter	Value	Comments
Cell Power	90 [W]	Single Cell Power: 90[W] Cell Number: 60 Total Stack Power: 5.4 [kW]
Voltage	0.67 [V]	
Current Density	2000 [A/m ²]	
FU	85%	
Air excess ratio	4	
Fuel flow	0.099 [kg/sec]	0.002 [mol/sec]
Air flow	0.44 [kg/sec]	0.012 [mol/sec]

SOFC model to meet the average current density and 85% fuel utilization requirements. In addition, the tubular system is known for operating with lower air excess ratios due to the ability of the tubes in tolerating thermal gradients [14]. Hence, a relatively low air excess of four was chosen for the SOFC operation. The key cell operation variables at the design point are summarized in Table 4.

4 Modeling and Integration of SOFC/GT System

This section describes the modeling work on the turbomachinery part of the two SOFC/GT hybrid systems in single- and dual-shaft configurations. The SOFC nominal operating conditions shown in Table 4 are used as a baseline model for the sizing of gas turbines to match the SOFC design.

4.1 Single-Shaft GT. The GT model incorporates the shaft rotational speed dynamics, the compressor and the turbine sub-models. The performance data used in this study is specified in the form of compressor and turbine maps [15], which present absolute values for a specific compressor. Since no map of commercially available turbines matched the specifications of the mass flow and pressure ratios required by the SOFC/GT under investigation, the maps used in this modeling work, shown in Fig. 5, were derived by normalization and proper scaling. The main variables used in those models include pressure p , flow \dot{m} , temperature T and power P . Note that the subscripts denote the component (c for compressor and t for turbine) and the inlet or outlet (1 or 2, respectively). For example, p_{c2} denotes the outlet pressure of the compressor.

These compressor and turbine maps provide steady-state mass flow, pressure ratio, and efficiency as a function of turbine rotational speed. The mass flow can be calculated from the performance maps for any given rotational speed, pressure ratio. Once the mass flow is determined, a compressor efficiency can be determined from the efficiency map. Knowing the isentropic efficiency, the compressor exit temperature can be determined from the isentropic relations described as follows:

$$T_{c2} = T_{c1} \left\{ 1 + \frac{1}{\eta_{comp}} \left[\left(\frac{p_{c2}}{p_{c1}} \right)^{\frac{\gamma-1}{\gamma}} - 1 \right] \right\} \quad (6)$$

The power P_c required to drive the compressor can be related to the mass flow rate \dot{m}_c and the enthalpy change across the compressor from the first law of thermodynamics as

$$P_c = \dot{m}_c (h_{c2} - h_{c1}) \quad (7)$$

Assuming that the specific heat coefficients of air do not change, we have

$$P_c = \dot{m}_c c_{p,c} (T_{c2} - T_{c1}) \quad (8)$$

The turbine model is constructed in a similar way as the compressor. The turbine/generator rotational dynamics are determined by

the power generated by the turbine, P_t , the power required to drive the compressor P_c and the power drawn by the generator P_{gen} as:

$$\frac{dN}{dt} = \frac{P_t \eta_m - P_c - P_{gen}}{\alpha \cdot N \cdot J} \quad (9)$$

Where N is the turbine speed in rpm and η_m is the turbine mechanical efficiency that accounts for energy losses due to friction. The turbocharger inertia is considered constant and equal to a typical value of 0.95. The turbocharger inertia J is the sum of rotor inertia, compressor inertia and turbine wheel inertia about the axis of rotation. The factor $\alpha = (2\pi/60)^2$ is a result of converting the speed from rad/s to revolutions per minute (rpm).

In addition, in modeling the catalytic burner (CB), the mass/temperature dynamics used in Ref. [9] are taken into account as follows:

$$\frac{dm_{cb}}{dt} = W_{ca} + W_{an} - W_t, \quad (10)$$

$$m_{cb} c_{p,cb} \frac{dT_{cb}}{dt} = \sum_{k=1}^n N_{k,cb}^{In} h_{k,cb}^{In} - \sum_{k=1}^n N_{k,cb}^{Out} h_{k,cb}^{Out} \quad (11)$$

where W_{ca} , W_{an} are the anode and cathode outlet mass flows, respectively, and W_t is the flow through the turbine. $h_{k,cb}^{In}$, $h_{k,cb}^{Out}$ are the inlet and outlet enthalpies of the gas species k and $N_{k,cb}^{In}$, $N_{k,cb}^{Out}$ are the associated molar inflow and outflow rates.

4.2 Dual-Shaft GT. The model for the dual shaft system is developed following the same modeling guidelines used for the single-shaft design. The dual-shaft turbine maps are resized properly so that the dual-shaft turbine power matches that of the single-shaft system at the design point. The same equations are used to calculate the inlet/outlet temperatures and enthalpies for the twin-shaft GT modeling. The rotor dynamics of gas and power turbines are modeled as in Eqs. (12) and (13), respectively,

$$\frac{dN_1}{dt} = \frac{P_{t,1} \eta_{m,1} - P_c}{\alpha \cdot N_1 \cdot J_1} \quad (12)$$

$$\frac{dN_2}{dt} = \frac{P_{t,2} - bN_2^2 - P_{gen}}{\alpha \cdot N_2 \cdot J_2} \quad (13)$$

where b is the friction coefficient of the power turbine. Contrary to Eq. (12), the damping effect due to the mechanical friction is represented in a separate form (bN_2^2) which yields a stable damped response of the power turbine. Since these two turbines have no mechanical coupling, the design offers flexibility in operating the compressor and the generator at different speed to achieve optimal efficiency.

5 Steady-State Performance Evaluation

In this section, we first calculate the steady state operation regimes for the two different design options. Three control variables are varied independently within their respective limits. Each combination determines an output power and an operation point of the system.

5.1 Operation Envelopes. Figure 6 show the steady-state operation ranges for a single- and dual-shaft SOFC/GT hybrid model, respectively. Steady state operation exists only in the dark-shaded areas. The power ranges of two designs are very close: 3.0– 6.0kW for the single-shaft design and 3.0–5.7kW for the dual-shaft design. This is because the SOFC has been built up under the same design condition and the turbines have been modeled to produce a similar power at the 100% rpm for the comparison study purpose. For the single shaft system, the efficiency varies from 32.0% to 42.6%, while for the dual shaft, a narrower range of efficiency window is observed for its entire operating

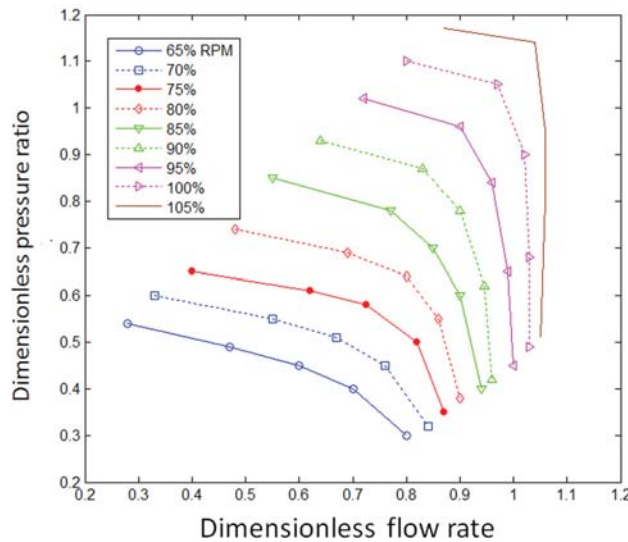
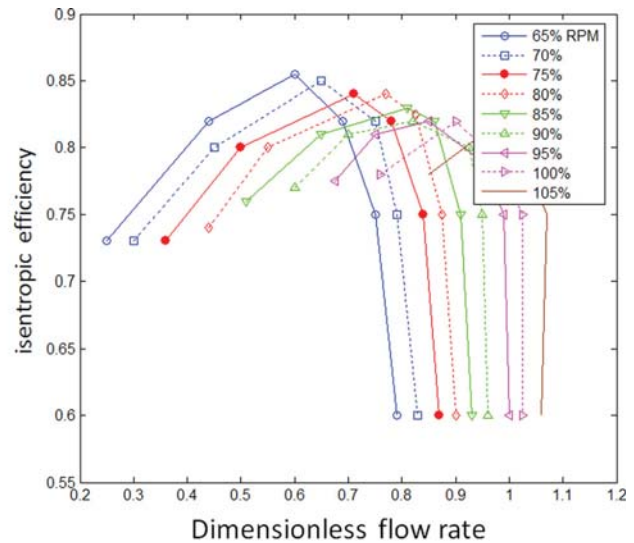


Fig. 5 Normalized performance map for a compressor. It is based on a generic map from Ref. [15].



range, namely, from the lowest 32.0% to the highest 39.2%. The dual-shaft hybrid system show slightly better part-load performance than the single-shaft system does. The efficiency values are plotted along the boundary lines of the operation regimes depicted in Fig. 6. The efficiencies are higher in the lower boundary points of the turbine power (P_{Turb}) and the shaft speed (N) while the low efficiencies are found in the lower boundaries of the SOFC temperature (T_{CELL}) and the generator load (P_{GEN}). For the high fuel flow and low P_{GEN} combination, which is outside the shaded area on the low efficiency side, the turbine speed is steadily climbing far beyond the operating ranges (overspeed) and the fuel cell is also over cooled and therefore the voltage is expected to be low. On the other hand, the cause of infeasible operation related to the other extreme end (low fuel flow, high P_{GEN}) is due to the fuel/air starvation in the fuel cell stack along with the high SOFC temperature limitation.

The single-shaft design has a wider operation range than that of the dual shaft as shown in the plots of Fig. 6. This is because in the dual-shaft model, the compressor pressure ratio is shared by the gas- and power-turbines. The decrease in the turbine power is mainly due to the less pressure ratio applied to one stage in the dual-shaft configuration. Besides, the single-shaft design has a higher power split ratio (P_{GEN}/P_{NET}) compared with the dual-shaft design. Figure 7 shows that a power split ratio for the single-shaft design varies over 7%–8% while that of a dual-shaft design is nearly 2%. The reduced turbine power generation range in the dual-shaft model leads to the decrease in the power split ratio. In dual-shaft design, the lower/upper boundaries of P_{GEN} are almost flat over the entire P_{NET} region. In contrast, the upper boundary of the P_{GEN} in the single-shaft design decreases by more than 50% from the maximum P_{GEN} . This means that the small (large) generator load variation is expected for the dual (single)-shaft design, when a load is changed along the high efficiency boundary line.

Given the large thermal time constant and the delicacy of the SOFC units, it might be desirable to keep the SOFC at a constant operating condition even when the load demand has been changed. Figure 8 presents the load operation range while a constant SOFC output power is maintained. The load variation over a fixed SOFC power is very limited (± 0.3 kW) and uniform over the entire P_{NET} range for both single- and dual-shaft cycles. This analysis shows that using SOFC as the base power plant and the generator for load following is not a feasible strategy for this class of SOFC/GT system.

SOFC cell temperature is another practical constraint, as it affects reliability and lifetime of the cell, as well as the system efficiency. Maintaining relatively high-level of SOFC temperature can be made possible in the high load operation regime, (e.g.,

1040 K can be achieved in the region of $P_{NET} \geq 5.0$ kW in the single design and $P_{NET} \geq 5.2$ kW in the dual design as seen from Fig. 6). In addition, based on the steady state performance data, operating the system at a constant SOFC temperature for different load condition seems feasible for certain load operation range. The largest load operation range for which the P_{NET} can vary while the temperature is kept constant is found between 4.0–5.5 kW in the single-shaft design, see the upper plot in Fig. 9. However, for the dual shaft counterpart, this range becomes narrower and is almost constant regardless the load condition (see the lower plot in Fig. 9), which indicates that a single shaft design is more favorable for the part-load operation under a constant SOFC temperature constraint. It is also noticeable that maintaining a constant shaft speed is doable over the entire load interval for both the single- and dual-shaft designs.

5.2 Analysis of Part-Load Operation. In this section, the system part-load behavior is investigated. The strategies for part-load operation and for effective transition from one operation point to another are discussed.

5.2.1 Single-Shaft SOFC/GT Design. The operation of SOFC/GT plants is dictated by three different control inputs, namely the fuel flow, the SOFC current density, and the generator power. Therefore, there exist multiple ways of achieving a prescribed load following objective. This study investigates load change schemes to explore the control design space that can achieve fast and safe load following operation. To illustrate the concept and the analysis method, we consider two load points with $P_{NET} = P_A$ and $P_{NET} = P_B$. By analyzing the feasible input regimes for each operating point and the overlap in the two corresponding regions, we gain insight on how to achieve efficient part load operation while facilitating fast load following. As a representative example, the feasible input setpoints matching the powers of 5.0 kW (P_A) and 5.7 kW (P_B) are calculated as displayed in Fig. 10 for the single-shaft design. The crucial system variables such as the fuel cell temperature, system efficiency, and the shaft speed are shown in the operating area. The areas highlighted in Fig. 10(b)–10(d) indicate that the combination of the corresponding inputs can generate the specified powers. The white area represents input points that cannot meet the power demand. Major observations and findings concerning the load operation are summarized as follows:

Regions of feasible control inputs: It is clear that as P_{NET} increases from lower power (5.0 kW) to a higher power (5.7 kW), the entire operating regime shifts in the fuel flow W_{Fuel} and the SOFC current density (I_{COM}) plane such that more power from the

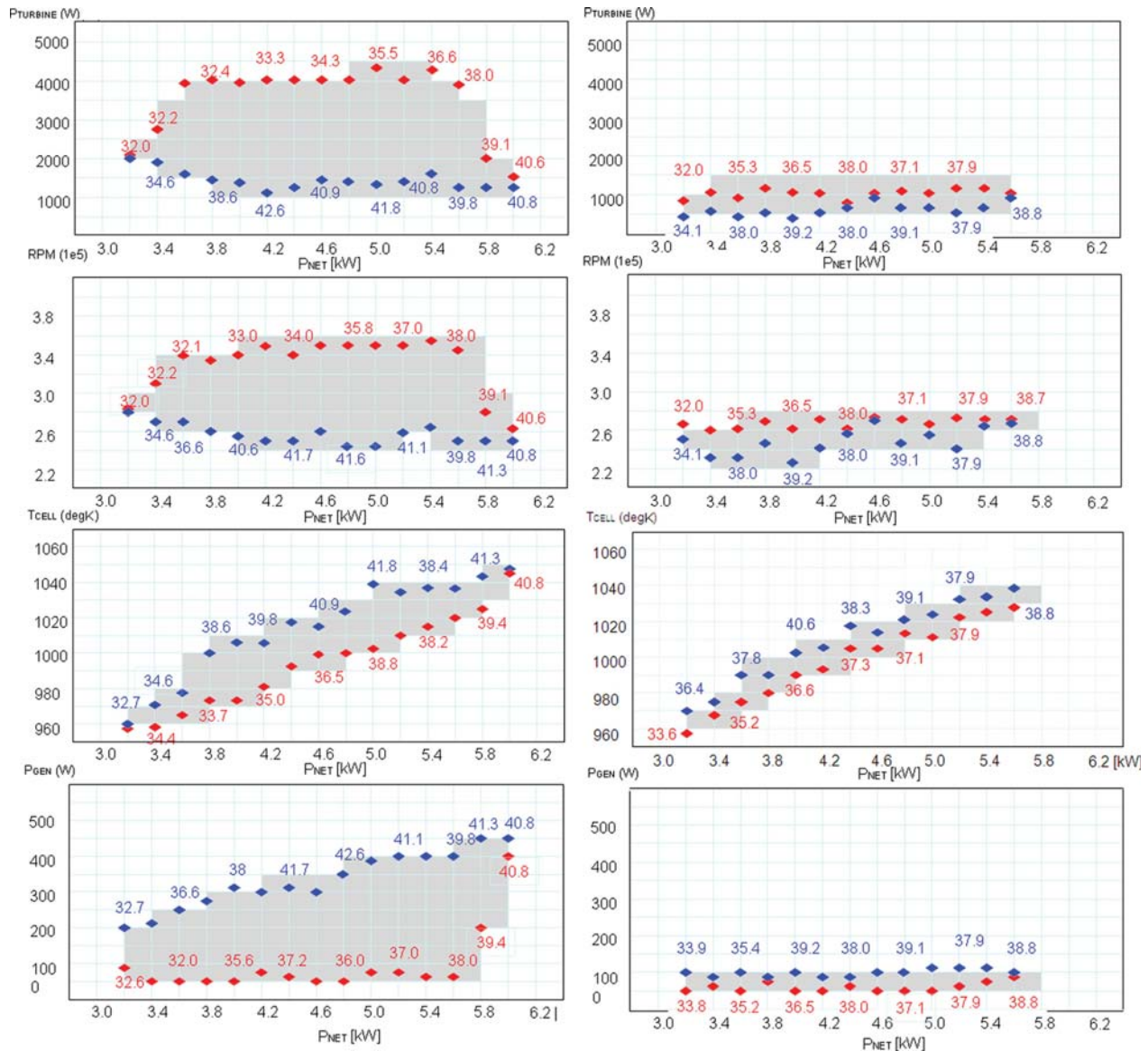


Fig. 6 Steady-state operating regimes of a single (LHS) and dual-shaft (RHS) SOFC/GT cycle: Turbine power, shaft speed, fuel cell temperature, and generator load. The efficiency data are plotted along the upper and lower boundaries of the feasible operating region.

fuel cell stack can be produced. This is the case with both single- and dual-shaft designs. Note that at a constant net power, the efficiency is inversely proportional to the fuel flow since $\eta = P_{NET} / (W_{Fuel} \cdot LHV)$ and thus the corresponding fuel flows at the power

of 5.0kW and 5.7kW can be readily calculated from the efficiency data of Fig. 10(b) for the entire feasible operating range. Note that the diagonal distribution of the feasible region is due to the fact that $P_{NET} = P_{FUEL}(I_{COM}) + P_{GEN}$. Outside this region, either too much (upper right area) or not enough (lower left) power will be produced.

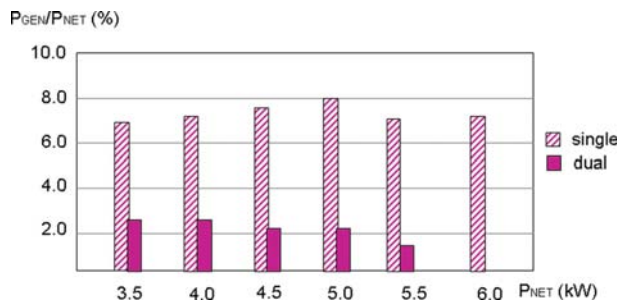


Fig. 7 Comparison of power split ratios for single- and dual-shaft designs

Sensitivity of part load efficiency to control variables: From Fig. 10(b), it is observed that high efficiency setpoints are located in the upper boundary of the operating regime while low efficiency setpoints are situated in the lower boundary line. The setpoints associated with $\eta = 39\%$ for the 5.0kW power are spread out most widely along the operation regimes and the range of the feasible operation is shrinking as η increases. In particular, P_{GEN} increases while I_{COM} tends to decrease as η reaches its maximum of 41%. The reduction in I_{COM} can be attributed to the fact that the low fuel supply increases the chance of the fuel starvation in the fuel channel and thus limiting the operating range of I_{COM} . On the other hand, in case an excessive fuel flow enters the fuel cell, the gas turbine overspeeding can occur. Note that the lowest efficiency points are positioned where P_{GEN} value is near

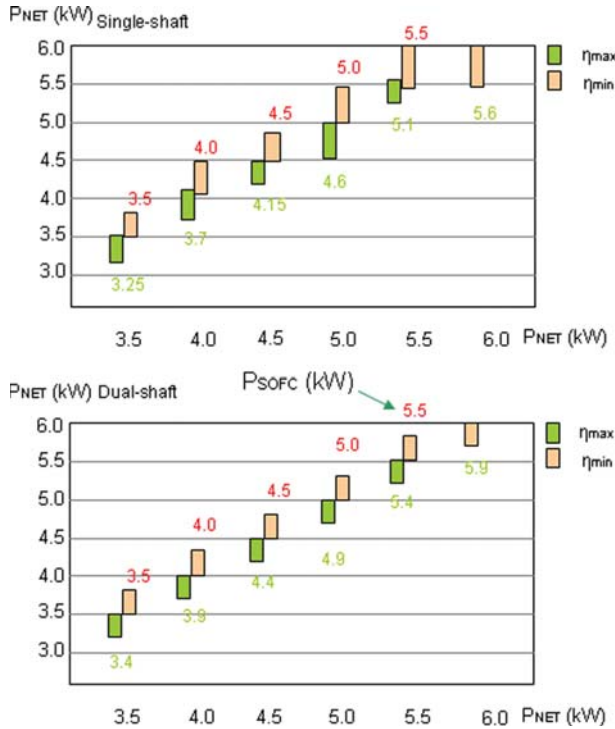


Fig. 8 Operating envelope with SOFC power constraints: Single-shaft (upper plot) and dual-shaft (lower plot). The numbers on the plots indicate the output power of the SOFC.

to zero and the SOFC current values are relatively high. In summary, the high efficiency of the hybrid system under study can be achieved if the operation can be sustained under a low fuel flow, a low fuel cell current, and a high generator load. In other words, maximizing the power split ratio P_{GEN}/P_{NET} under the constraint of $P_{NET} = P_{FUEL}(I_{COM}) + P_{GEN}$ is the way of achieving the high efficient operation. This observation reveals the fact that the selection of P_{GEN} as a control variable cannot only expand the operating region, but also make significant contribution to achieve a high efficiency of the SOFC/GT hybrid system.

Temperature and turbine speed variation analysis: From the performance maps in Fig. 10(c), the fuel cell temperature tends to increase when the generator load and the SOFC current are set to be high and the fuel flow to be low. In this control setting, more heat is generated from the electrochemical process and the less air cooling effect is applied to the fuel cell. The operating domains of the fuel cell temperature for the set powers of 5.0kW and 5.7kW are computed to be [1002,1020]deg K and [1025,1048]deg K, respectively. This means that with the load change from 5.0kW to 5.7kW, maintaining constant cell temperature is not likely to happen. However, minimizing the fuel cell temperature variation can be achieved by well coordinated input combinations. In this particular example, the setpoints from $(\eta, I_{COM}, P_{GEN}) = (39.5, 1750, 350)$ at 5.0kW to $(38.9, 2100, 300)$ at 5.7kW leads to the smallest fuel cell temperature variation of 5 K. It is also noticeable that in case of a load increase operation, keeping constant fuel cell temperature and achieving high efficiency are competing requirements, the cell temperature deviation can be minimized at the cost of the system efficiency. However, in case of load decrease scenario, the two-fold purpose to achieve the high efficiency and minimal fuel cell temperature change is achievable. It should be noted that the result depends on both the magnitude and direction of load change. The shaft speed varies uniformly over an interval of $[2.57, 3.59] \times 10^5$ rpm for the power of 5.0kW and $[2.60, 2.84] \times 10^5$ rpm for the power of 5.7kW, indicating that part-load operation with a constant speed is possible. However, varying the speed of the gas turbine can provide greater flexibility in turbine operation.

5.2.2 Dual-Shaft SOFC/GT Design. The performance analysis for a dual-shaft SOFC/GT cycle has been also conducted with respect to the performance critical factors, such as the fuel cell temperature and the efficiency, and the results are shown in Fig. 11. The plots show the feasible setpoints of the efficiency (Fig. 11(a)) and fuel cell temperature (Fig. 11(b)) for two output power level of 5.0kW and 5.7kW, respectively. It is shown that the current density and the fuel flow increase as the power level increases from 5.0kW to 5.7kW (refer to Table 5 for the fuel flow variation). The fuel cell temperature is also increased since more heat is generated at the high power of 5.7kW. Even though the two-shaft design of the hybrid SOFC/GT cycle is advantageous in mechanical design because of its simplicity, the operating range is considerably smaller in comparison to the single-shaft configuration as shown in Fig. 11. The load change from 5.0kW to 5.7kW in the dual shaft configuration leads to less changes in the fuel cell temperature and the turbine shaft speed than the single-shaft configuration. For example, the efficiency gap between 5.0kW and 5.7kW in the dual shaft design is only 0.8% compared to 3.3% in the single-shaft design, the temperature gap is 10 K less in comparison to the single-shaft cycle. Due to the low power split ratio, the variable speed in the dual-shaft design exhibits the uniform part load efficiency.

Table 5 compares the admissible ranges of the three independent control variables at the two different power levels. The operation windows associated with the fuel flow and the SOFC current density at 5.0kW and 5.7kW are completely separated, while there is much overlap among the feasible intervals of the generator load for both single- and dual-shaft systems.

As shown in Fig. 10, under a constant fuel flow (see $\eta = 41\%$ at 5.0kW in Fig. 10), the temperature increases as the fuel cell current (generator load) increases (decreases). This suggests that between the two competing factors, namely (a) increase in SOFC current increases the temperature and (b) decrease in generator load decreases the temperature, the former is more dominant. However, the generator load shows a very attractive feature that it can exert constant influence on the SOFC temperature at the different power levels. For example, the temperature differences attributed to the generator load variations in the middle value of

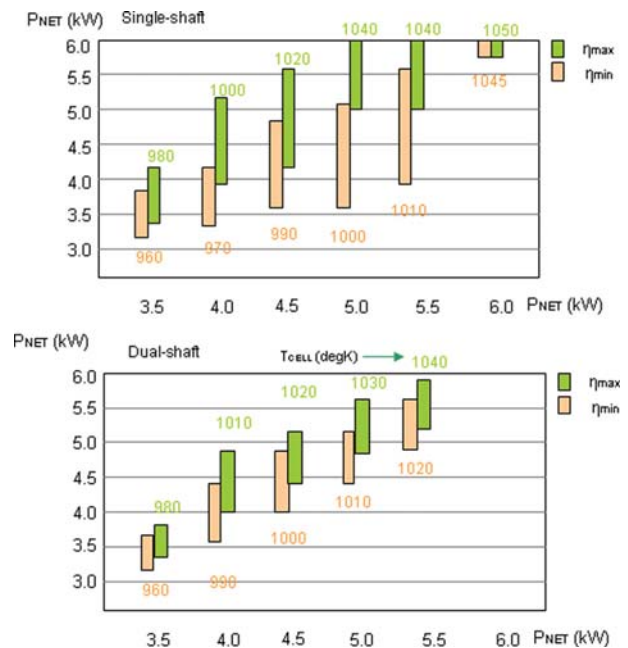


Fig. 9 Operating envelope with temperature constraints: Single-shaft (upper plot) and dual-shaft (lower plot). The numbers shown on the plots are cell temperature T_{CELL} in deg K.

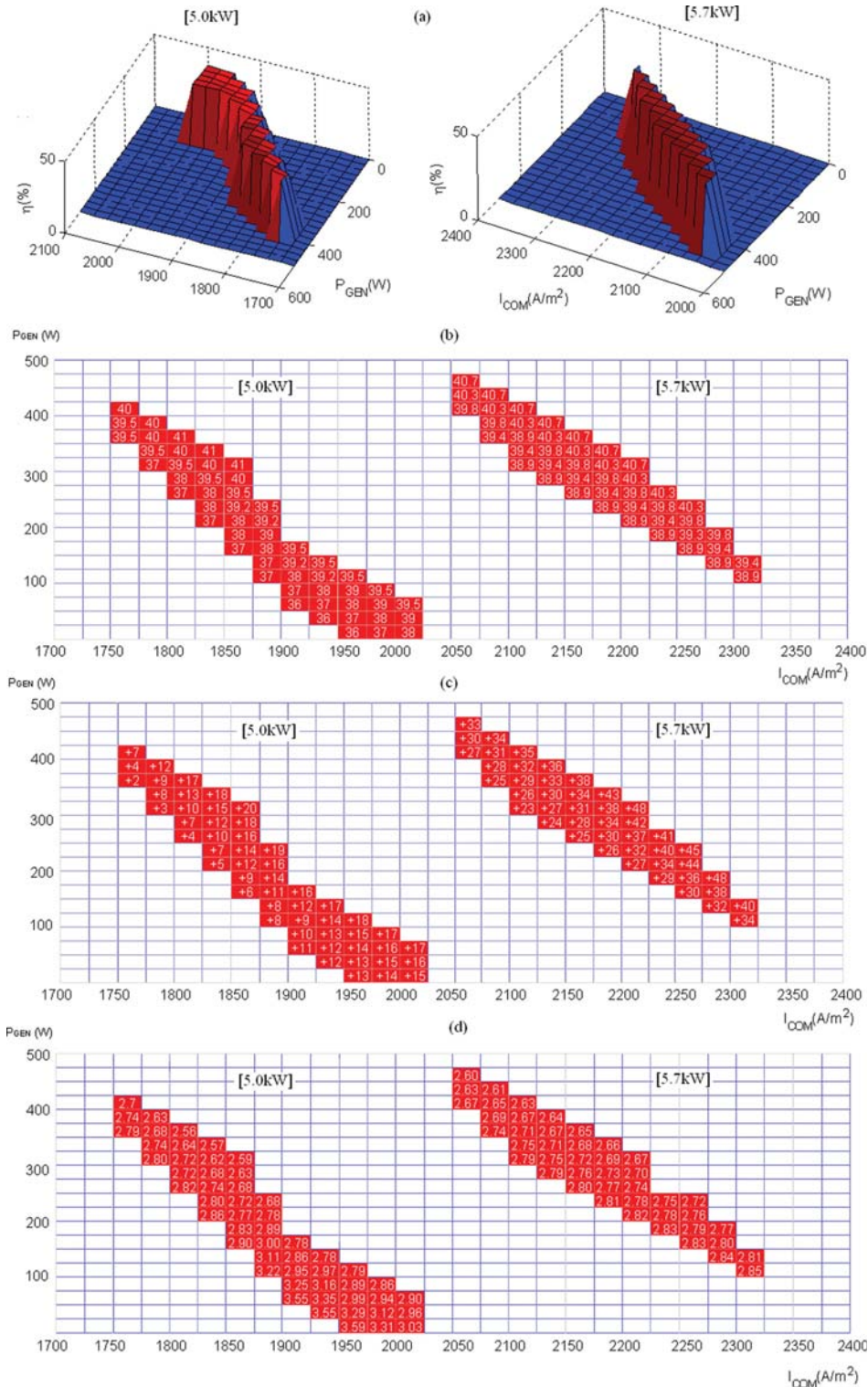


Fig. 10 The single-shaft operating regime to produce the net powers of 5.0kW and 5.7kW. (a),(b) system efficiency 3D/2D maps, (c) fuel cell temperature variation at 1000 K, (d) shaft speed ($\times 10^5$) as functions of SOFC current density and a generator load.

an SOFC current are 14 K at the power of 5.0kW and 13 K at the power level of 5.7kW. Hence, in case the SOFC current and fuel flow are designated as controlling variables for the power control objective as claimed by Ref. [14], the generator load can be utilized as an alternative control element for an SOFC temperature management.

6 Dynamic Performance Evaluation

It has been established that the hybrid SOFC/GT system is susceptible to shutdown when a sudden load increase is applied [9]. In this analysis, we use the operating envelope identified earlier to characterize the shutdown mechanism for two different SOFC/GT configurations. The region of attraction (ROA), a notion used to

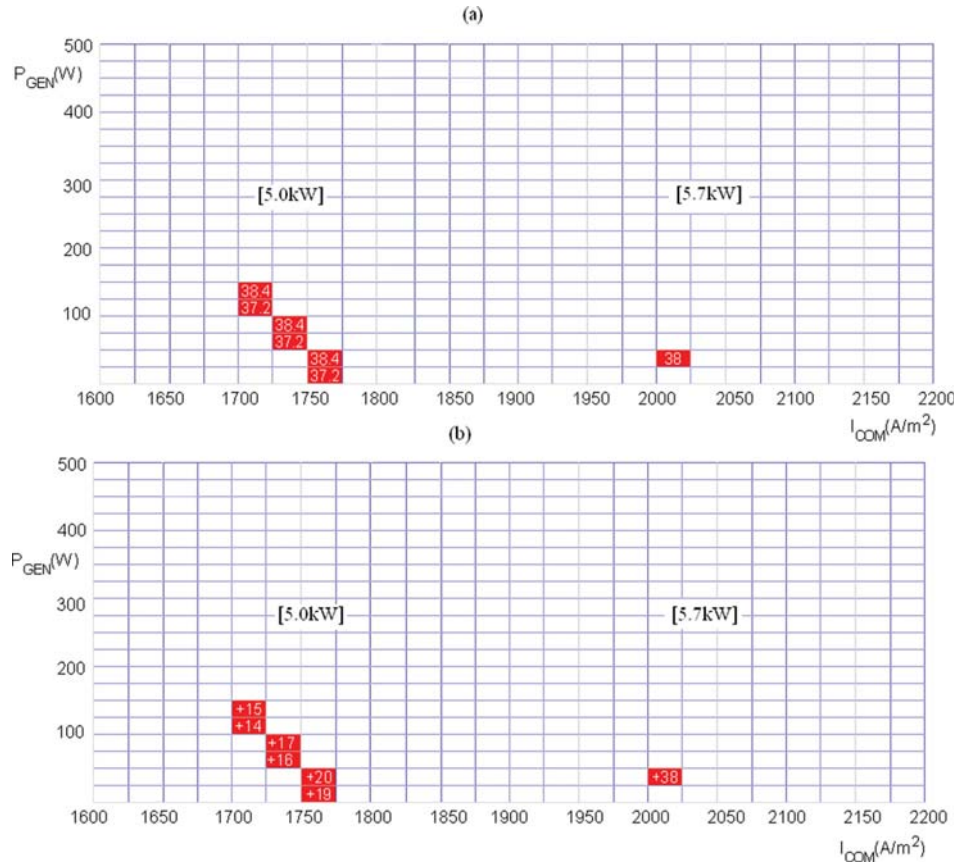


Fig. 11 The dual-shaft operating regime to produce the net powers of 5.0kW and 5.7kW. (a) system efficiency, (b) fuel cell temperature as functions of a generator load and a SOFC current density.

characterize the stability of a nonlinear system is used in this paper to elucidate the stability properties of the SOFC/GT. For a given operating point and associated equilibrium, the ROA is defined as the set of all initial states from which the trajectories will converge to the steady state equilibrium point.

6.1 Shutdown Problem. In this section, the ROAs of two SOFC/GT models are identified and analyzed for the shutdown phenomenon. We denote $x_{ss}(P_{NET})$ and $ROA(P_{NET})$ as the steady state and region of attraction respectively for a given power demand PNET. Then the ROA provides a numerical tool to capture and understand the shutdown phenomenon. For example, consider the case that the system is settled at an equilibrium point $x_{ss}(P_A)$, but it is required to step up the power to P_B with $P_A < P_B$, the system will shutdown if

$$x_{ss}(P_A) \notin ROA(P_B) \quad (14)$$

On the other hand if

$$x_{ss}(P_A) \in ROA(P_B) \quad (15)$$

the system can reach the new desired equilibrium

The ROAs are computed in terms of three dominant states, namely the fuel cell temperature, the CB mass, and the shaft speed, as investigated in the previous study [9]. The three dimensional region of attraction corresponding to $P_{NET} = 5.7\text{kW}$ with input settings $(W_{Fuel}, I_{COM}, P_{GEN}) = (0.002, 2100, 390)$ is sketched on two dimensional planes (with the cell temperature and CB mass as two axes) as the shaded areas in Fig. 12 for four different shaft speeds. From the region of attraction boundaries it can be

seen that if the initial condition for the mass and the rotational speed is high, then the required initial condition for the temperature is lowered. This trend can be explained by noting that the higher the initial temperature, mass, and rotational speed are, the higher turbine power is. The energy provided to the GT shaft increases as temperature, mass and rotational speed increase. Thus; for example, to reach the stable equilibrium starting at low mass, low rotational speed and $P_{NET} = 5.7\text{kW}$, the temperature has to be high in order to make up for the energy needed to support the load on the GT shaft.

To illustrate a situation when system shutdown occurs, three load operation scenarios are evaluated in the single-shaft SOFC/GT system as shown in Table 6. S_1, S_3, S_4 are operation points with the highest efficiency for their specified powers of 4.6/5.0/5.7 kW while S_2 is the lowest efficiency point at the power of 4.6 kW. In case of a small step load change from 5.0 kW (S_3) to 5.7 kW (S_4), it can be shown that the equilibrium point of 5.0 kW (S_3) resides within the ROA of 5.7 kW with a large margin to the lower boundary line. On the other hand, consider two larger

Table 5 The control variables' distribution matching the net powers of 5.0 kW and 5.7 kW

Turbine type	Input	5.0 kW	5.7 kW
Single	W_{Fuel}	$[1.7, 1.95] \times 10^{-3}$	$[2.2, 1] \times 10^{-3}$
	I_{COM}	[1679, 1909]	[1955, 2185]
	P_{gen}	[0, 420]	[120, 480]
Dual	W_{Fuel}	$[1.6, 1.65] \times 10^{-3}$	1.8×10^{-3}
	I_{com}	[1700, 1750]	2000
	P_{gen}	[0, 150]	25

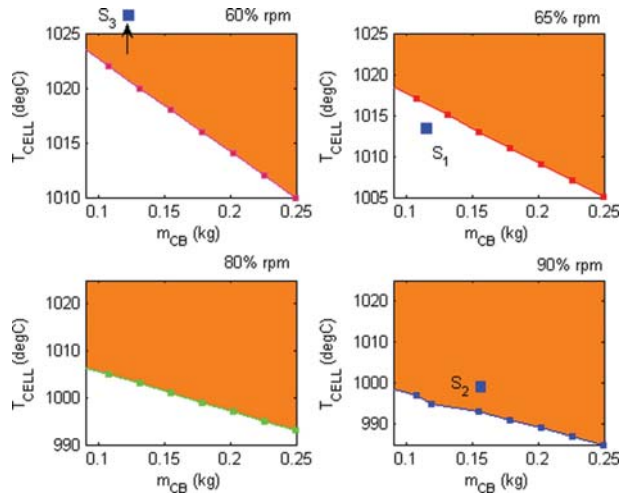


Fig. 12 ROA sketch for a single-shaft SOFC/GT model with a net power of 5.7kW and input setting $(W_{FUEL}, I_{COM}, P_{GEN}) = (0.002, 2100, 390)$. The ROA of a SOFC temperature and a CB mass are computed under four different initial turbine shaft speeds. The equilibrium point is $(rpm, T_{CELL}, m_{CB}) = (65\% \text{ rpm}, 1039^\circ\text{C}, 0.117\text{kg})$.

step load maneuvers from 4.6kW($S_1; S_2$) to 5.7kW(S_4). Note that S_1 and S_2 differ in that S_1 is optimized for efficiency while S_2 is not. The equilibrium point with 4.6kW(S_1) falls slightly outside of the ROA of 5.7kW as shown in Table 6(65%rpm) while that of S_2 is located above the lower boundary of the ROA. This means that the load change from 4.6kW(S_1) to 5.7kW(S_4) leads the system to shutdown while the other two operations, namely $S_2 \rightarrow S_4$ and $S_3 \rightarrow S_4$ transient are sustainable.

The analysis can be validated by the simulation when the demanded load power steps, from $P_{net} = 4.6/5.0\text{kW}$ to $P_{net} = 5.7\text{kW}$, are applied without feedback control. The input settings, identified from the previous section, are used to change the fuel flow, the current, and the generator power as listed in Table 6. It is observed that the system shuts down after the steps are applied from 4.6kW(S_1) to 5.7kW(S_4) at $t = 2000\text{sec}$. During the

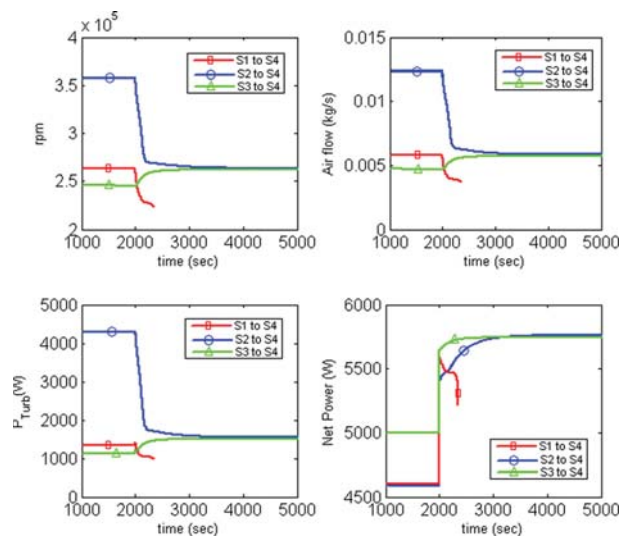


Fig. 13 Load step response of a single shaft SOFC/GT system from 4.7 kW TO 5.7 kW under highest (S_1, S_3, S_4)/lowest S_2 efficiency setpoints for current density, fuel, and generator load as a function of load

Table 6 The load operation points to illustrate the shutdown behavior of single- and dual-shaft SOFC/GT systems. Note: Input = $[W_{Fuel} \text{ (kg/s)}, I_{com} \text{ (A/m}^2\text{)}, P_{GEN} \text{ (W)}]$, State = $[rpm(\%), T_{cel}(\text{deg K}), m_{CB} \text{ (kg)}]$

P_{NET}	Single
4.6 kW	$S \rightarrow$ Input: (0.0016,1800,200) $S \rightarrow$ State: (65,1016,0.127) $S_2 \rightarrow$ Input: (0.0019,1750,0) $S_2 \rightarrow$ State: (90,1002,0.151)
5.0 kW	$S_3 \rightarrow$ Input: (0.0017,1900,350) $S_3 \rightarrow$ State: (60,1038,0.124)
5.7 kW	$S_4 \rightarrow$ Input: (0.002,2100,390) $S_4 \rightarrow$ State: (65,1039,0.117)
P_{NET}	Dual
4.6 kW	$D_1 \rightarrow$ Input: (0.00175,1750,100) $D_1 \rightarrow$ State: (65,1014,0.147)
5.0 kW	$D_2 \rightarrow$ Input: (0.00185,1850,100) $D_2 \rightarrow$ State: (67,1017,0.148)
5.7 kW	$D_3 \rightarrow$ Input: (0.0021,2000,50) $D_3 \rightarrow$ State: (67.0,1042,0.153)

4.6kW(S_1) to 5.7kW(S_4) step, the immediate increase in the generator load deprives the turbine from having enough power to supply the air during the transient to support SOFC operation, causing the turbine shaft to stall and eventually the system to shut down. On the contrary, when a load switches from 4.6kW(S_2) or 5.0kW(S_3) to 5.7kW(S_4), the system shutdown does not occur due to the sufficient initial kinetic energy in the turbine and thermal energy in the SOFC exhaust.

A dual-shaft gas turbine design has been also studied to examine the operating characteristics and the load following performance for a SOFC/GT. We consider an open-loop response when a net power switches from 4.6kW(D_1)/5.0kW(D_2) to 5.7kW(D_3) which is the same load change conditions as those used in the single-shaft model analysis. The corresponding input settings are $(W_{FUEL}, I_{COM}, P_{GEN}) = (0.00175, 1750, 100)_{D1}$, $(0.00185, 1850, 100)_{D2}$, and $(0.0021, 2000, 50)_{D3}$, which offer the highest efficiency set points at the powers of 4.6/5.0/5.7kW, respectively. Figure 14 depicts that both

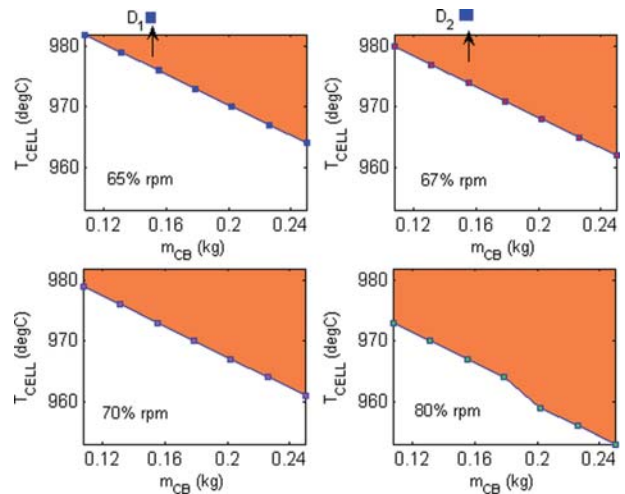


Fig. 14 ROA lower boundary for a dual-shaft SOFC/GT model for $P_{NET} = 5.7\text{kW}$ and $(W_{FUEL}, I_{COM}, P_{GEN}) = (0.0021, 2000, 50)$. The equilibrium point is $(rpm, T_{CELL}, m_{CB}) = (67\% \text{ rpm}, 1042^\circ\text{C}, 0.15\text{kg})$.

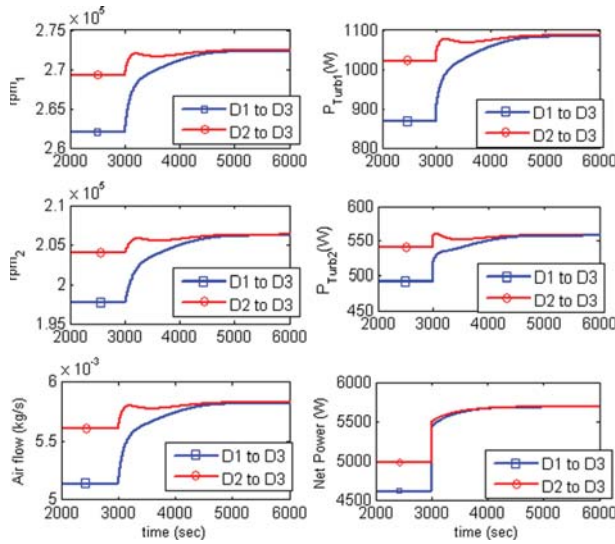


Fig. 15 System responses of a dual shaft SOFC/GT during a step from 4.6kW to 5.7kW, namely $D_1 \rightarrow D_3$ and $D_2 \rightarrow D_3$. The same conditions as the single-shaft model simulation have been used.

equilibrium points of 4.6kW(D_1) and 5.0kW(D_2) are contained in the ROA at the power of 5.7kW(D_3). Therefore, no shutdown is observed in Fig. 15. In contrast to the single-shaft load change case of 4.6kW \rightarrow 5.7kW, one can notice that the small amount of the generator power (50W) is applied due to the low power split ratio and thereby the dual-shaft SOFC/GT becomes less vulnerable to the system shutdown under aggressive load change.

7 Conclusions

This study has examined the characteristics of the SOFC/GT hybrid cycles from the fundamental operating regime to the part load performance. Two different mechanical designs are assumed: dual shaft and single shaft as the compressor turbine connection mechanism. The analysis leads to the following conclusions: First, the single-shaft design provides wide operation envelopes compared to the dual shaft operation when the same compressor model is employed in the SOFC/GT system. The gap between the operation ranges stems from their mechanical designs, as the compressor discharge pressure in a dual-shaft design has to be shared by two turbines of a turbocharger and thus the power split ratio of the dual shaft SOFC/GT becomes much smaller than that of the single-shaft design. The dual shaft cycle would require a higher compressor pressure ratio to achieve the operating envelope to be comparable to the conventional single-shaft design. Furthermore, the system efficiency is less sensitive to the load in part load operation in the dual shaft design in comparison to the single-shaft cycle. Second, turbine shaft speed control through a generator load manipulation in both SOFC/GT configurations can be effective in enhancing the part load efficiency and maintaining the fuel cell temperature variation at its minimal. However, its usefulness is more pronounced in a single-shaft design. Third, through model based simulations, it was demonstrated that the optimal steady state setpoints lie on the boundary of the admissible operation region and thus the use of optimal steady state setpoints for load transitions makes the system susceptible to transient issues and imposes the need for advanced control schemes. By analyzing the region of attraction, the responses to the load change of the dual-shaft model has been proved to be more robust against the shutdown problem than its single-shaft counterpart. The dynamic load response could be further improved by using more advanced model-based controllers. This is a part of ongoing research.

Acknowledgment

This work is funded in part by U.S. Army TARDEC and in part by U.S. Navy under NEEC (Naval Engineering Education Center).

Nomenclature

- $C_{(·)}$ = concentration of species (·) (mol/m³)
- c_p = heat capacity (J/kg·K)
- $d_{\eta a}$ = hydraulic diameter of the fuel/air channel
- F = Faraday's constant (C/mol)
- $h_{(·)}$ = gas enthalpy of species (·) (J/kg)
- I = shaft inertia (kg m²)
- I_{COM} = current density (A/m²)
- L = cell length (cm)
- m = mass (kg)
- N = shaft rotational speed (rpm)
- $N_{in/out,i}$ = inlet/outlet molar rate of species i (mol/s)
- $N_{U,i}$ = Nusselt number of channel i
- $p_{(·)}$ = pressure of (·) (Pa)
- $P_{(·)}$ = power of (·) (kW)
- $r_{SR/WGS/O_2}$ = rate of reaction (mol/s·m [2])
- R = universal gas constant (J/K·mole)
- R_{Ohm} = cell resistance ($\Omega \cdot m^2$)
- s_p = cell pitch/2
- T = temperature (K)
- U = voltage (V)
- V = volume (m³)
- \dot{m} = flow (kg/s)
- $\epsilon_{PEN/INJ}$ = PEN/injector emissivity
- λ_{PEN} = PEN thermal conductivity (J/m · s · K)
- λ_{air} = air ratio
- $\nu_{s,·}$ = stoichiometric coefficient of species s
- $\rho_{PEN/INJ}$ = PEN/injector density (kgm⁻³)
- σ = Stefan-Boltzmann constant (W/m² · K⁴)
- σ_{An} = anode electrical conductivity (1/ $\Omega \cdot m$)
- $\tau_{An/El/Ca}$ = anode/electrolyte/cathode thickness (m)

References

- [1] Singhal, S. C., and Kendall, K., 2003, *High Temperature Solid Oxide Fuel Cells*, Elsevier, New York.
- [2] Campanari, S., 1998, "Power Plants Based on Solid Oxide Fuel Cells Combined With Gas Turbine Cycles," Ph.D. dissertation, Polytechnic University of Milan, Milan, Italy.
- [3] Larminie, J., and Dicks, A., 2004, *Fuel Cell System Explained*, Wiley, New York.
- [4] Palsson, A., Selimovic, A., and Sjunnesson, L., 2000, "Combined Solid Oxide Fuel Cell and Gas Turbine Systems for Efficient Power and Heat Generation," *J. Power Sources*, **86**, pp. 442–448.
- [5] Roberts, R. A., and Brouwer, J., 2006, "Dynamic Simulation of a Pressurized 220kW Solid Oxide Fuel-Cell Gas-Turbine Hybrid System: Modeled Performance Compared to Measured Results," *J. Power Sources*, **3**, pp. 18–25.
- [6] Roberts, R. A., Brouwer, J., Jabbari, F., Junker, T., and Ghezal-Ayagh, H., 2006, "Control Design of an Atmospheric Solid Oxide Fuel Cell/Gas Turbine Hybrid System: Variable Versus Fixed Speed Gas Turbine Operation," *J. Power Sources*, **161**, pp. 484–491.
- [7] Wang, X., Huang, B., and Chen, T., 2007, "Data-Driven Predictive Control for Solid Oxide Fuel Cells," *J. Process Control*, **17**, pp. 103–114.
- [8] Wchter, C., Lunderstdt, R., and Joos, F., 2006, "Dynamic Model of a Pressurized SOFC/Gas Turbine Hybrid Power Plant for the Development of Control Concepts," *J. Fuel Cell Sci. Technol.*, **3**, pp. 271–279.
- [9] Tsourapas, V., 2007, "Control Analysis of Integrated Fuel Cell Systems with Energy Recuperation Devices," Ph.D. thesis, University of Michigan.
- [10] Oh, S.-R., and Sun, J., 2010, "Optimization and Load-Following Characteristics of Skw-Class Tubular Solid Oxide Fuel Cell/Gas Turbine Hybrid Systems," American Control Conference, Baltimore, MD, pp. 417–422.
- [11] Xi, H., 2007, "Dynamic Modeling and Control of Planar SOFC Power Systems," Ph.D. thesis, University of Michigan.
- [12] Aguiar, P., Adjiman, C. S., and Brandon, N. P., 2004, "Anode-Supported Intermediate Temperature Direct Internal Reforming Solid Oxide Fuel Cell. I: Model-Based Steady-State Performance," *J. Power Sources*, **138**, pp. 120–136.
- [13] Hall, D. J., 1997, "Transient Modeling and Simulation of a Solid Oxide Fuel Cell," Ph.D. dissertation, University of Pittsburgh, PA.
- [14] Stiller, C., Thorud, B., Seljebo, S., Mathisen, O., Karoliussen, H., and Bolland, O., 2005, "Finite-Volume Modeling and Hybrid-Cycle Performance of Planar and Tubular Solid Oxide Fuel Cells," *J. Power Sources*, **141**, pp. 227240.
- [15] Stiller, C., Thorud, B., and Bolland, O., 2005, "Safe Dynamic Operation of a Simple SOFC/GT Hybrid System," *Proceedings of the 2005 ASME Turbo Expo*, Reno, NV.